Formation of Electromagnetic Postsolitons in Plasmas

N. M. Naumova,[1,2,*] S. V. Bulanov,[2] T. Zh. Esirkepov,[3] D. Farina,[4] K. Nishihara,[5]
F. Pegoraro,[6] H. Ruhl,[1] and A. S. Sakharov[2]
[1]*Max-Born-Institut, Berlin, Germany*
[2]*General Physics Institute of RAS, Moscow, Russia*
[3]*Moscow Institute of Physics and Technology, Dolgoprudny, Russia*
[4]*Istituto di Fisica del Plasma, CNR, Milano, Italia*
[5]*Institute of Laser Engineering, Osaka University, Osaka, Japan*
[6]*Department of Physics, Pisa University and INFM, Pisa, Italia*
(Received 15 April 2001; published 16 October 2001)

With particle-in-cell simulations we show that electromagnetic relativistically strong solitons, formed in the wake of the laser pulse during the interaction of a high-intensity ultrashort laser pulse with a collisionless plasma, evolve asymptotically into postsolitons. A postsoliton is a slowly expanding cavity in the ion and electron densities which traps electromagnetic energy. Fast ions are accelerated during the postsoliton formation. Postsolitons are elementary components of the relativistic electromagnetic turbulence in laser-irradiated plasmas.

DOI: 10.1103/PhysRevLett.87.185004 PACS numbers: 52.38.–r, 52.35.Sb, 52.65.Rr

When a relativistically intense laser pulse propagates in a plasma, dispersion effects come into play due to the finite inertia with which electrons respond to the electromagnetic (e.m.) fields, while the nonlinearity appears due to the relativistic increase of the electron mass and to the plasma density redistribution under the action of the ponderomotive force. This force pushes the plasma particles (the electrons first and, at a later time, the ions) away from the region of maximum e.m. field. These effects lead to well-known nonlinear phenomena such as relativistic self-focusing [1] and relativistic e.m. soliton generation. The analytical theory of relativistic e.m. solitons has been developed in Refs. [2–7]. Relativistic solitons have been seen in multidimensional particle-in-cell (PIC) simulations of the laser pulse interaction with a plasma [8–10]. In Ref. [4] fast solitons propagating in the plasma with group velocity close to the speed of light were invoked as a tool for particle and photon acceleration.

The theory of these solitons has been developed mainly within the framework of the approximation of immovable ions. When the ion dynamics is taken into account, solitons have been found to exist just at propagation velocities larger than a critical velocity [7]. On the other hand, PIC simulations [8] demonstrated that the solitons are generated in the wake left behind the laser pulse and they propagate with a velocity that is well below the speed of light and that in a homogeneous plasma is almost equal to zero. The time of the soliton formation is much shorter than the ion response time so that ions can be assumed to be at rest during the soliton formation. Ions can be assumed to be at rest during approximately $(m_i/m_e)^{1/2}$ oscillation periods of the e.m. field inside the soliton (the period of the field oscillation inside the soliton is of the order of $2\pi\omega_{pe}^{-1}$). For longer times the ponderomotive pressure of the e.m. field inside the soliton starts to dig a hole in the ion density, and the parameters of the soliton change. Rigorously speaking, what was a soliton on the electron time scale ceases to be a soliton on the ion time scale. Nevertheless, a low frequency e.m. wave packet remains in the plasma, being well confined inside the slowly expanding plasma cavity. We call this nonlinear e.m. wave packet a "postsoliton." It is important to know the properties of postsolitons because in an underdense plasma a substantial part of the laser pulse energy can be converted into solitons [8–10] which afterwards evolve into postsolitons.

The aim of this paper is to show for the first time, with the help of 2D3V (all quantities depend on the x and y coordinates and on time and the particle momenta have three components) PIC simulations, the basic properties of the postsoliton in collisionless plasmas.

In the simulations presented here the size of the simulation box is 30λ along x (the direction of the laser pulse propagation) and 30λ along y (transverse direction). The cell size is $1/16 \times 1/16\lambda^2$ with nine electrons and nine ions per cell. The total number of particles is approximately 3×10^6. The plasma begins at $x = 5$ and is preceded by a vacuum region 5λ long. The normal incident laser pulse is initialized outside the plasma in the vacuum region $x < 0$. In the run shown here, the dimensionless amplitude of the laser radiation is $a = eE/m\omega c = 1$ (which corresponds to the intensity $I \approx 1.37 \times 10^{18}$ W/cm^2 for a 1 μm wavelength pulse). The laser pulse has a Gaussian form both in the x and in the y directions, with full width $l_\perp = 5\lambda$ and length $l_\parallel = 4\lambda$, corresponding to a 13.3 femtosecond pulse length at 1 μm wavelength, and is linearly s polarized (i.e., with its incident electric field along the z axis). In the simulations presented here, the ion mass is $1836m_e$. The plasma density is $n_0 = 0.36n_{\rm cr}$, where $n_{\rm cr} = \omega^2 m/4\pi e^2$ is the critical density. The corresponding ratio between the plasma period and the period of the laser radiation is 1.67. Between the plasma and the vacuum regions there is an exponential density ramp 5λ long.

The evolution in the (x, y) plane of the z component of the electric field (first column) and of the electron and ion densities (second and third columns) at $t = 30$, 70, and 120 is shown in Figs. 1(a)–1(c). Here, and in the following, the time and space coordinates are measured in laser periods and wavelengths, respectively, the electron and ion densities in units of the initial density, and the electric field in units of $m\omega c/e$.

In the distribution of the z component of the electric field at time $t = 30$, we see the laser pulse, which has changed its form due to the nonlinear processes, the scattering of the e.m. radiation, and the formation of an s-polarized e.m. soliton of the type considered in Refs. [8–10]. The laser pulse changed its shape due to nonlinear processes such as self-focusing and energy depletion. The formation of the soliton, as discussed in Ref. [9], is related to the trapping of the e.m. energy due to the pulse frequency downshift caused by the pulse depletion. The soliton is seen at the center of the computation region. In the distribution of the electron density we see a local minimum in the position of the soliton and no substantial modulation in the ion density distribution. In the distribution of the electron density we also see the modulations due to excitation of the wakefield behind the laser pulse near the pulse axis in the region $10 < x < 15$ and a bunch of fast electrons at $x = 22.5$, $y = 0$. However, the wakefield generation and the electron acceleration do not influence the soliton significantly. At time $t = 70$, after the remnants of the pulse have left the simulation box, we see the postsoliton that remains at the place where the soliton was formed. During its evolution the postsoliton radiates away a portion of its energy in the form of an e.m. wave. The electric field inside the soliton oscillates periodically, changing its sign as in the case of electron solitons discussed in Refs. [9,10]. The hole in the electron density becomes wider and we see a hole in the distribution of the ion density with almost the same radius as that of the electron hole. The largest density corresponds to the rings at the boundary of the postsoliton. Figure 1(c) shows the asymptotic structure of the postsoliton at time $t = 120$. The postsoliton has a perfect circular form, aside from the effect of the interaction with the wakefield. The radius of the hole in the electron and ion densities increases. The width of the density ring becomes larger. We see a small scale structure inside the ring, which corresponds to three confocal rings.

In Fig. 2(a) we show the distribution of the z component of the electric field and in Fig. 2(b) we show the ion density inside the postsoliton at $t = 120$.

We can describe the scenario of the postsoliton formation as follows. Since the soliton formation time is much shorter than the ion response time $\approx 2\pi(m_i/m_e)^{1/2}\omega_{pe}^{-1} = 2\pi\omega_{pi}^{-1}$, ions can be assumed to be at rest during the soliton formation. Inside the nonpropagating soliton (half-cycle soliton [6]) the maximum of the e.m. field a_m and the soliton frequency ω_s are connected as $a_m = 2(\omega_{pe}^2 - \omega_s^2)^{1/2}/\omega_s$ and the soliton width is equal to $c/(\omega_{pe}^2 - \omega_s^2)^{1/2}$. The ponderomotive pressure of the e.m. field inside the soliton is balanced by the force due to the electric field which appears due to charge separation. The amplitude of the resulting electrostatic potential is given by $\phi = (1 + a_m^2)^{1/2}$. The ponderomotive pressure displaces the electrons outward and the Coulomb repulsion in the electrically non-neutral ion core pushes the ions away. The typical ion kinetic energy corresponds to the electrostatic

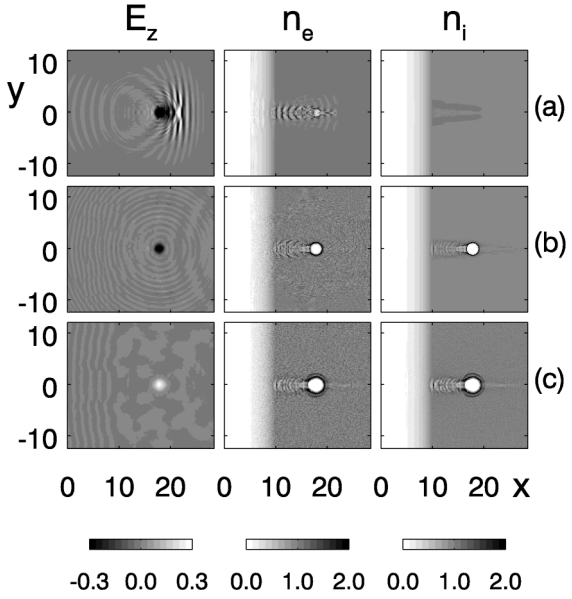

FIG. 1. Interaction of an s-polarized laser pulse with the plasma: the z component of the electric field (left column), the electron density (middle column), and the ion density (right column) in the x, y plane at $t = 30$ (a), $t = 70$ (b), and $t = 120$ (c).

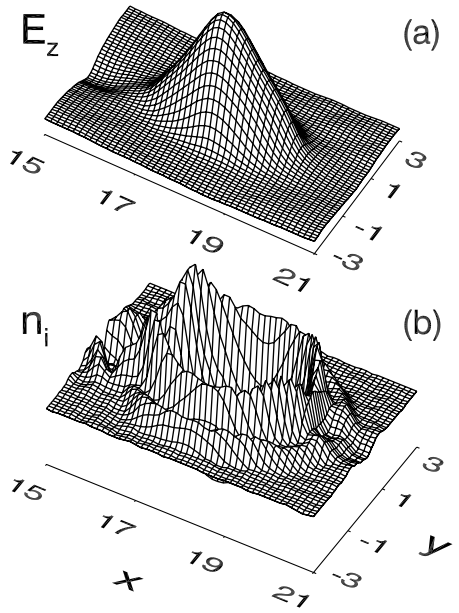

FIG. 2. 3D plot of the z component of the electric field (a) and of the ion density (b) inside the postsoliton at $t = 120$.

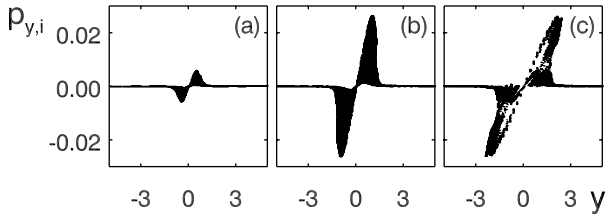

FIG. 3. The ion phase plane (p_y, y) inside the postsoliton at $x = 18$, $y = 0$ for $t = 30$ (a), 70 (b), and 120 (c).

potential energy which is of the order of $m_e c^2 a_m$. This process is similar to the so-called "Coulomb explosion" inside self-focusing channels (see Ref. [11]).

In Fig. 3 we show the ion phase plane (p_y, y) at $t = 30$, 70, and 120. We see that the radial component of the momentum of the fastest ions does not depend on time for $t > 30$. The fastest ions are located at the outermost ring seen in the ion density distribution in Fig. 1.

The ion expansion in the radial direction leads to the digging of a hole in the ion density. The cavity formation in the distribution of the electron and ion densities is shown in Figs. 1 and 4. In Fig. 4(a) the e.m. energy density distribution at $x = 18$ is shown versus y at $t = 30$, 70, and 120, together with the electron (dotted line) and the ion (solid line) density distributions in Fig. 4(b). The plasma cavity forms a resonator for the trapped e.m. field. During the cavity expansion, the amplitude and frequency of the e.m. field decrease. Since the radius of the cavity increases very slowly compared to the period of the e.m. field oscillations, we can use the adiabatic approximation to find their dependence on time (see Ref. [12]). The adiabatic invariant in this case is the ratio between the energy and the frequency of the e.m. field:

$$\int \mathbf{E}^2 \, dV/\omega_s = \text{const}. \tag{1}$$

As a simple analytical model to describe the e.m. field inside the postsoliton, we can use the well-known electric- or magnetic-dipole oscillations inside a spherical resonator (see Ref. [12]), where the lowest frequency depends on the cavity radius as $\omega_s = 2.74c/R$, for the electric-dipole mode, and as $\omega_s = 4.49c/R$, for the magnetic-dipole mode. From Eq. (1) we find that $E^2 \sim R^{-4}$. Under the action of the e.m. pressure the wall of the cavity moves, piling up plasma as a snow plow. In the "snow plow" approximation [13] all the mass of the plasma pushed by the e.m. pressure $\langle \mathbf{E}^2 \rangle / 8\pi$ is located inside a thin shell. The mass inside the shell is equal to the mass M initially contained inside a sphere of the radius R: $M = 4\pi n_0 m_i R^3/3$. We write the second Newton's law for the motion of the mass M as

$$\frac{d}{dt}\left(M \frac{dR}{dt}\right) = 4\pi R^2 \frac{\langle \mathbf{E}^2 \rangle}{8\pi}, \tag{2}$$

or, using the expressions $M = 4\pi n_0 m_i R^3/3$ and $\langle \mathbf{E}^2 \rangle = \langle \mathbf{E}_0^2 \rangle (R_0/R)^4$, in the form

$$\frac{d}{dt}\left(R^3 \frac{dR}{dt}\right) = \frac{3R_0^4 \langle \mathbf{E}_0^2 \rangle}{8\pi n_0 m_i R^2}. \tag{3}$$

Here E_0 is the amplitude of the electric field inside the soliton, which evolves into the postsoliton, and $R_0 \approx c/\omega_{pe}$ is the soliton radius. By integrating Eq. (3), we obtain

$$\frac{R}{R_0} = \left[\frac{(2\tau^2)^{2/3} + (2\tau^2 + t^2 + t\sqrt{4\tau^2 + t^2})^{2/3}}{(2\tau^2)^{1/3}(2\tau^2 + t^2 + t\sqrt{4\tau^2 + t^2})^{1/3}} - 1 \right]^{1/2}, \tag{4}$$

where the time scale of the cavity expansion is equal to $\tau = \sqrt{6\pi R_0^2 n_0 m_i / \langle \mathbf{E}_0^2 \rangle}$. Asymptotically, when $t \to \infty$, the postsoliton radius increases as $R \approx R_0 (2t/\tau)^{1/3}$; the amplitude of the e.m. field and its frequency decrease as $E \sim t^{-2/3}$ and $\omega_s \sim t^{-1/3}$. Similarly, in the case of the cylindrical cavity, we find that $R \sim t^{2/5}$, when $t \to \infty$.

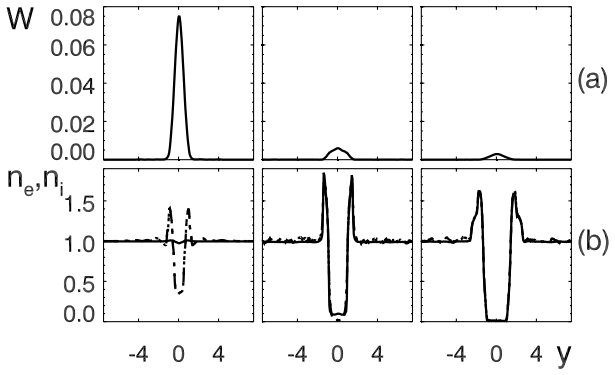

FIG. 4. Cuts of the e.m. energy density distribution (a) and of the electron (dash-dotted line) and ion (solid line) densities normalized on n_0 (b) at $t = 30$, 70, and 120.

In Fig. 5(a) we present the log-log plot of the dependence of the cavity radius versus time, as obtained from the simulation. Although the above estimates are rather rough, as they do not take into account the inner structure of the shell, we see that this dependence is nevertheless in fairly good agreement with the $R \sim t^{2/5}$ law. The time dependence of the maximum positive value of the z

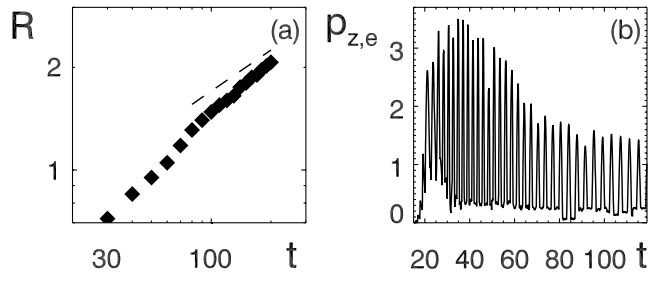

FIG. 5. Dependence of the logarithm of the cavity radius on the logarithm of time (a); time dependence of the maximum positive value of momentum along z of different electrons inside the postsoliton (b).

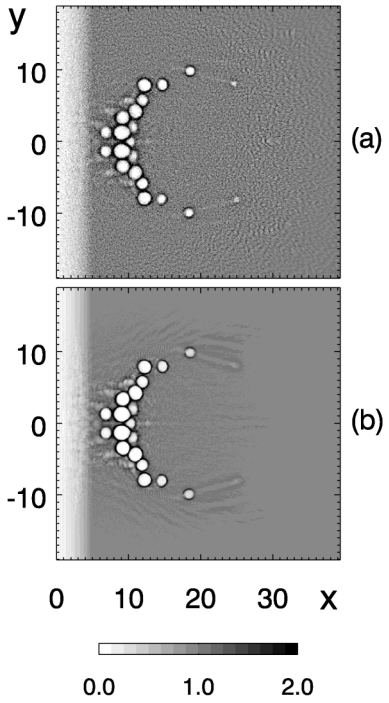

FIG. 6. Distribution of the electron (a) and ion (b) density in the (x, y) plane showing the postsoliton necklace formed behind a wide laser pulse at $t = 70$.

component of the momentum of different electrons inside the postsoliton is plotted in Fig. 5(b). The band at the bottom of the figure is due to electron heating. We see that the amplitude and frequency of oscillations decrease in time. Thermal effects do not contribute to the cavity evolution because the quiver momentum is substantially larger than the thermal momentum. However, later in time the plasma pressure can become of the order of the ponderomotive pressure inside the cavity and stop its expansion.

Wider laser pulses produce a cloud of solitary waves in their wake [9]. When the ponderomotive pressure of the e.m. field inside the solitons starts to dig holes in the ion density the soliton cloud evolves into postsolitons, as shown in Fig. 6 for an s-polarized pulse with amplitude $a = 1$, width 30λ, and length 15λ in an underdense plasma ($n/n_{\rm cr} = 0.64$) at $t = 70$. In the distribution of the electron [Fig. 6(a)] and ion densities [Fig. 6(b)] we see a "necklace" of the postsolitons.

In conclusion, when a relativistically strong e.m. wave propagates in a plasma, a portion of its energy is transformed into solitons which then form slowly expanding cavities in the distribution of the ion and electron densities with the e.m. field trapped inside. The regular structures seen in the ion distribution in the postsoliton necklace in the laser field can be a source of high harmonic emission and fast ion generation.

We are pleased to acknowledge the use of the Cray T3E supercomputing facility at the Konrad-Zuse-Zentrum für Informationstechnik Berlin (ZIB).

*Electronic address: http://staff.mbi-berlin.de/naumova

[1] A. G. Litvak, Sov. Phys. JETP **30**, 344 (1969); C. Max *et al.,* Phys. Rev. Lett. **33**, 209 (1974); G. Schmidt and W. Horton, Comments Plasma Phys. Control. Fusion **9**, 85 (1985); P. Sprangle *et al.,* IEEE Trans. Plasma Sci. **PS-15**, 145 (1987); A. B. Borisov *et al.,* Phys. Rev. A **45**, 5830 (1992).

[2] J. I. Gersten and N. Tzoar, Phys. Rev. Lett. **35**, 934 (1975); N. L. Tsintsadze and D. D. Tskhakaya, Sov. Phys. JETP **45**, 252 (1977).

[3] V. A. Kozlov *et al.,* Sov. Phys. JETP **49**, 75 (1979).

[4] K. Mima *et al.,* Phys. Rev. Lett. **57**, 1421 (1986); P. K. Kaw *et al.,* Phys. Rev. Lett. **68**, 3172 (1992).

[5] T. Tajima and T. Taniuti, Phys. Rev. A **42**, 3587 (1990); T. Kurki-Suonio, P. J. Morrison, and T. Tajima, Phys. Rev. A **40**, 3230 (1989).

[6] T. Zh. Esirkepov *et al.,* JETP Lett. **68**, 36 (1998); D. Farina *et al.,* Phys. Rev. E **62**, 4146 (2000).

[7] D. Farina and S. V. Bulanov, Phys. Rev. Lett. **86**, 5289 (2001); Plasma Phys. Rep. **27**, 680 (2001).

[8] S. V. Bulanov *et al.,* Phys. Fluids B **4**, 1935 (1992).

[9] S. V. Bulanov *et al.,* Phys. Rev. Lett. **82**, 3440 (1999).

[10] Y. Sentoku *et al.,* Phys. Rev. Lett. **83**, 3434 (1999).

[11] G. S. Sarkisov *et al.,* Phys. Rev. E **59**, 7042 (1999); T. Zh. Esirkepov *et al.,* JETP Lett. **70**, 82 (1999); S. V. Bulanov *et al.,* JETP Lett. **71**, 407 (2000); Y. Sentoku *et al.,* Phys. Rev. E **62**, 7271 (2000); K. Krushelnik *et al.,* Phys. Plasmas **7**, 2055 (2000).

[12] L. D. Landau and L. M. Lifshits, *Electrodynamics of Continuous Media* (Pergamon, Oxford, 1984).

[13] Ya. B. Zel'dovich and Yu. P. Raizer, *Physics of Shock Waves and High-Temperature Hydrodynamic Phenomena* (Academic, New York, 1967).